

Effects of Radiative Transfer Modeling on Transient Temperature Distribution in Semitransparent Glass Rod

Zhiyong Wei

e-mail: gte384w@prism.gatech.edu

Kok-Meng Lee

e-mail: kokmeng.lee@me.gatech.edu

Serge W. Tchikanda

The George W. Woodruff School of Mechanical Engineering,
Georgia Institute of Technology,
Atlanta, GA 30332-0405

Zhi Zhou

e-mail: zhizhou@ofsoptics.com

Siu-Ping Hong

e-mail: shong@ofsoptics.com

OFS,
Norcross, GA 30071

This paper presents a method of modeling the radiative energy transfer that takes place during the transient of joining two concentric, semitransparent glass cylinders. Specifically, we predict the two-dimensional transient temperature and heat flux distributions to a ramp input which advances the cylinders into a furnace at high temperature. In this paper, we discretize the fully conservative form of two-dimensional Radiative Transfer Equation (RTE) in both curvilinear and cylindrical coordinate systems so that it can be used for arbitrary axisymmetric cylindrical geometry. We compute the transient temperature field using both the Discrete Ordinate Method (DOM) and the widely used Rosseland's approximation. The comparison shows that Rosseland's approximation fails badly near the gap inside the glass media and when the radiative heat flux is dominant at short wavelengths where the spectral absorption coefficient is relatively small. Most prior studies of optical fiber drawing processes at the melting point (generally used Myers' two-step band model at room temperature) neglect the effects of the spectral absorption coefficient at short wavelengths ($\lambda < 3 \mu\text{m}$). In this study, we suggest a modified band model that includes the glass absorption coefficient in the short-wavelength band. Our results show that although the spectral absorption coefficient at short wavelengths is relatively small, its effects on the temperature and heat flux are considerable. [DOI: 10.1115/1.1565081]

Keywords: Computational, Cylinder, Heat Transfer, Radiation, Transient

1 Introduction

The manufacture of optical fibers often requires joining two concentric glass cylinders, in which the partially joined cylinders initially at room temperature are moved into the furnace at a temperature typically in the neighborhood of the glass melting temperature (between 1500 K to 2500 K). Since the glass conductivity is very small, radiation is the dominant mode of heat transfer. During the transient, sufficiently large temperature gradient could result in cracking at the interface. As direct measurement of the temperature field is often impossible, the design and control of the joining process has been accomplished by extensive trial-and-error methods. The ability to predict the thermally induced stresses caused by the transient heating offers a means to optimize the design and improve process speed, which requires a good understanding of the transient temperature distribution. In this paper, numerical methods are developed to predict the transient temperature field and its gradient within the semitransparent glass.

An accurate prediction of the temperature distribution depends on the solution method, and the approximation of the models describing the radiative properties of the medium for a given set of boundary conditions. Over the past two decades, a number of researchers have investigated methods to predict energy transport in glass processing, most notably in applications of optical fiber drawing. Because glass is semitransparent to radiation, emission and absorption exist throughout the medium. The simplest approach, perhaps, has been to assume the participating medium is optically thick (or commonly known as the Rosseland's approximation) such that the radiative energy contributions from the boundary and the far away portions of the medium can be neglected. Rosseland's optically thick approximation reduces the to-

tal radiative flux to a simple temperature diffusion term; an effective radiative conductivity can then be used. This approach has been used by a number of researchers (Paek and Runk [1]; Homsy and Walker [2]; Myers [3]; Choudhury et al. [4]) to reduce the overall problem to a more tractable form in modeling multi-dimensional radiative heat transfer in glass. Homsy and Walker [2] pointed out that the Rosseland's assumption would break down at the surface, but no method was suggested to correct for the errors. An alternative approach is to solve the radiative transfer and the energy equations simultaneously using numerical methods. Lee and Viskanta [5] investigated combined conduction and radiation in a one-dimensional glass layer. By comparing the discrete ordinate method and the Rosseland approximation method, Lee and Viskanta [5] concluded that the diffusion approximation greatly underpredicts the temperature and heat flux when the thickness or the opacity of the layer is small. In a different study, Yin and Jaluria [6] employed a zonal method to investigate the radiative exchange within the neck-down profile of a glass preform for an assumed radial temperature profile. Their simulation results suggested that Rosseland's approximation underestimates the heat flux only when the radial temperature variation within the preform is substantial as compared with the zonal method. In these studies, only steady state solutions were considered.

The solution to the radiative transfer equation requires an appropriate model to describe the spectral absorption coefficient of the glass medium. Myers [3] introduced a two-step band model to describe the spectral absorption coefficients of a fused silica glass, which has been commonly used in the prediction of radiative transfer in optical fiber drawing processes. Myers' band model neglects the absorption at short wavelengths ($\lambda < 3.0 \mu\text{m}$), which has a relatively small value about $0.001 \sim 0.3 \text{ cm}^{-1}$ for semitransparent glasses. However, the spectral intensity of a blackbody radiation given by Planck's function (see for example Modest [7])

Contributed by the Heat Transfer Division for publication in the JOURNAL OF HEAT TRANSFER. Manuscript received by the Heat Transfer Division June 3, 2002; revision received January 2, 2003. Associate Editor: J. P. Gore.

suggests that more than 60% of radiative energy concentrates in the band $0.2 \mu\text{m} \leq \lambda < 2.8 \mu\text{m}$ near the melting temperature range of glass (1500 K ~ 2500 K). The effects of radiation absorption could be considerable in this short-wavelength band, although the absorption coefficient is small. Since the values for the spectral absorption coefficient of fused-silica glass at temperatures near the softening point were not known, Myers' two-step band model has been based on data taken at room temperature. Recent experiments (Endrys [8]; Nijnatten et al. [9,10]) on typical glasses suggested that the absorption coefficient in the $2.8 \mu\text{m} \leq \lambda < 4.8 \mu\text{m}$ band near the melting temperature is generally 10~25% lower than that at a room temperature of 25°C.

In this paper, we use the discrete ordinate method (DOM) to analyze the radiative transfer during the transient stage as two partially joined, concentric glass cylinders are moved into the furnace. Jamaluddin and Smith [11] used the DOM to predict radiative transfer in gas flame in axi-symmetric cylindrical enclosures. They showed that the results for DOM with S_4 quadrature approximation was in good agreement with the experimental data, and that S_6 approximation did not provide significantly better predictions but required 60% more computer time. More recently, Lee and Viskanta [12] used DOM to predict the spectral radiative transfer in a condensed cylindrical medium and have obtained good agreement with the exact solutions. The main contributions of this paper are summarized as follows:

1. We present the radiation model and the solution method for predicting the two-dimensional transient temperature gradient in joining two concentric glass cylinders as they are advanced into a furnace at a high temperature. The model and solution method serve as a basis for the prediction of the thermally induced stress intensity factors at the tip of the interface.
2. Unlike prior works by others (Jamaluddin and Smith [11], Lee and Viskanta [12]), which used grid face areas in the discretized equation in orthogonal cylindrical coordinates system, we present the fully conservative form of the two-dimensional RTE in both curvilinear and cylindrical coordinates systems so that the numerical scheme can be used for arbitrary axisymmetric cylindrical geometries.
3. We compare the popularly used Rosseland approximation and the numerical DOM in solving RTE for a two-dimensional transient heat transfer problem. Chung et al. [13] compared the accuracy between the Rosseland and P-1 approximations. Since the P-1 approximation drops higher order terms of the Fourier series for intensities, deviation from the exact solution (especially when the dimension of the glass is small) is considerable. Unlike prior comparison by Chung et al. [13] that consider steady-state one-dimensional glass layer for which the exact integration solution is available, this study offers additional insights for the two-dimensional cylindrical glass rod with an interior gap.
4. We show the considerable effect of spectral absorption coefficient at short wavelengths ($0.2 \mu\text{m} \leq \lambda < 2.8 \mu\text{m}$) in predicting the temperature field, which has been neglected in the previous studies on fiber draw process.

2 Analysis

Consider radiative transfer in a glass rod formed by a pair of concentric fused-silica glass cylinders as shown in Fig. 1. The gap between the two cylinders is very small as compared to the diameter of the cylinders. As the rod (initially at room temperature) is translated axially at a relatively slow, constant speed into a cylindrical furnace at a specified temperature profile, the cylinders become soft and join together at the gap. The interest here is to predict the transient temperature field of the glass rod as it enters the furnace. In addition, it is desired to determine the temperature gradient near the tip of the gap.

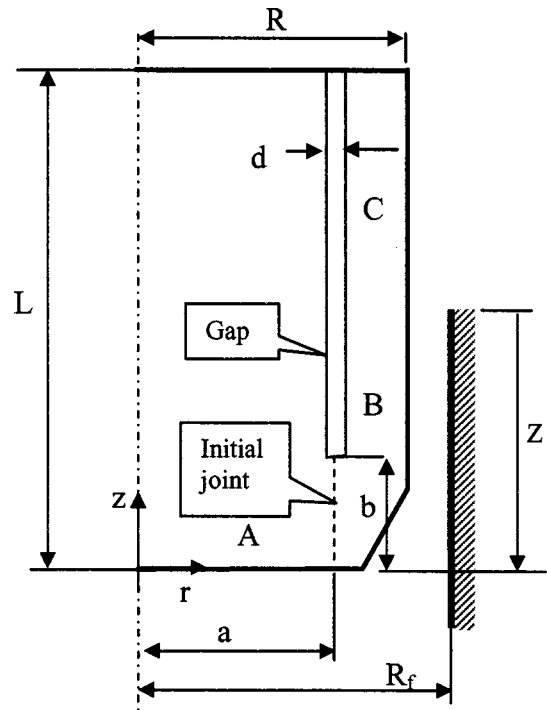


Fig. 1 Schematics illustrating the transient process

Glass is considered a homogeneous material, and scattering of radiation can be neglected in comparison to absorption and emission (Viskanta [14]). It is semitransparent to radiation in the spectral range $0 < \lambda < 5 \mu\text{m}$ and is almost opaque beyond $5 \mu\text{m}$. In addition, the following assumptions are made in the following formulation:

1. The system is axisymmetric and two-dimensional.
2. The refractive index of the medium is uniform and does not depend on temperature in the considered range.
3. The furnace walls are gray and diffuse.
4. We consider the case where the inner and outer surfaces at the glass interface and in the gap are diffuse for radiation reflection and transmission since the glass rod (called preform in industry) is not polished.
5. During the transient, the glass has not melted. The effects of the small deformation of the glass rod on the view factors can be neglected.

2.1 Formulation. The radiative transfer in a spectrally absorbing-emitting medium is modeled using the following radiative transfer equation (RTE):

$$\mathbf{s} \cdot \nabla I_\lambda(\mathbf{r}, \mathbf{s}) = \kappa_\lambda [n_\lambda^2 I_{b\lambda}(T) - I_\lambda(\mathbf{r}, \mathbf{s})] \quad (1)$$

where the spectral radiative intensity $I_\lambda(\mathbf{r}, \mathbf{s})$ is a function of the position vector \mathbf{r} , orientation vector \mathbf{s} , and wavelength λ ; $I_{b\lambda}(T)$ is the spectral intensity of a blackbody radiation given by Planck's function; κ_λ is the spectral absorption coefficient; and n_λ is the spectral index of refraction.

The divergence of the spectral radiation heat flux can be obtained by integrating Eq. (1) over the whole solid angle ($\Omega = 4\pi$), which yields

$$\nabla \cdot \mathbf{q}_\lambda = 4\pi \kappa_\lambda n_\lambda^2 I_{b\lambda}(T) - \kappa_\lambda \int_{\Omega=4\pi} I_\lambda(\mathbf{r}, \mathbf{s}) d\Omega \quad (2)$$

By solving the RTE for $I_\lambda(\mathbf{r}, \mathbf{s})$, the spectral radiative heat flux can be calculated from Equation (3):

$$\mathbf{q}_\lambda = \int_{\Omega=4\pi} I_\lambda(\mathbf{r}, \mathbf{s}) \mathbf{n} \cdot \mathbf{s} d\Omega \quad (3)$$

where \mathbf{n} is the normal vector of the surface. The corresponding total radiative heat flux is then given by

$$\mathbf{q} = \int_0^\infty \mathbf{q}_\lambda d\lambda \quad (4)$$

Since there is no glass flow during the transient, the energy equation for control volume fixed with the glass (no advection) only includes conductive and radiative heat transfer as shown in Eq. (5):

$$\rho C \frac{\partial T}{\partial t} = -\nabla \cdot (-k \nabla T + \mathbf{q}) \quad (5)$$

subject to the boundary conditions

$$\partial T / \partial r = 0 \quad \text{at } r = 0 \quad (5a)$$

$$-k \mathbf{n} \cdot \nabla T = q_{\text{rad,opa}} \quad \text{at the surface} \quad (5b)$$

where ρ , C , and k are the glass density, thermal capacity and conductivity, respectively; \mathbf{n} is the normal vector of the glass surface, $q_{\text{rad,opa}}$ is the net radiative flux at the opaque band on the glass surface. Natural convection of the air is neglected as compared with the radiative exchange.

The radiation intensity, through emission of the glass medium, depends on the temperature field and, therefore, cannot be decoupled from the overall energy equation. In addition, the solution to Eq. (1) depends on the approximation methods, the boundary conditions and the glass radiation properties. We discuss below two methods to solve for the transient temperature distribution; namely Rosseland approximation and a numerical scheme using the DOM.

2.2 Rosseland Approximation (RA). In the Rosseland's approximation (Modest [7]), the glass is assumed to be optically thick such that the radiative energy contributions from the boundary intensities and the far away portions of the medium are neglected. Thus, the total radiative flux can then be treated as a simple "radiative conduction" as follows:

$$\mathbf{q} \approx -\frac{16n^2\sigma T^3}{3\kappa_R} \nabla T = -k_{\text{rad}} \nabla T \quad (6)$$

where the Rosseland mean absorption coefficient κ_R can be evaluated from the integration of the spectral absorption coefficient with the weighting of $dI_{b\lambda}/dT$:

$$\frac{n^2}{\kappa_R} = \int_0^\infty \left(\frac{n_\lambda^2}{\kappa_\lambda} \right) \frac{dI_{b\lambda}}{dT} d\lambda \bigg/ \int_0^\infty \frac{dI_{b\lambda}}{dT} d\lambda \quad (7)$$

It can be seen that κ_R depends on temperature.

The radiative conductivity in Eq. (6) can be added to the molecule conductivity in the energy Eq. (5) to account for the radiative heat transfer. Although the RA results in extremely convenient form, it is worth noting that this diffusion approximation is not valid near a boundary and the optically thick assumption should be used with caution.

2.3 Numerical Computation Using DOM. The radiative intensities can be solved numerically from Eq. (1) using the DOM (Modest [7]). Once the intensities have been determined in each time step, the corresponding radiative heat flux inside the glass medium or at a surface can be solved from Eqs. (3) and (4), and the temperature distribution from the energy equation, Eq. (5).

2.3.1 Discrete Ordinate Equation. In the DOM, Eq. (1) is solved for a set of directions $\hat{\mathbf{s}}_i$, $i = 1, 2, \dots, N$. For an axisymmetric cylinder, the RTE along each of the N discrete directions can be expressed as

$$\frac{\mu^i}{r} \frac{\partial(rI_\lambda^i)}{\partial r} - \frac{1}{r} \frac{\partial(\eta^i I_\lambda^i)}{\partial \psi} + \xi^i \frac{\partial I_\lambda^i}{\partial z} = \kappa_\lambda [n_\lambda^2 I_{b\lambda}(T) - I_\lambda^i] \quad (8)$$

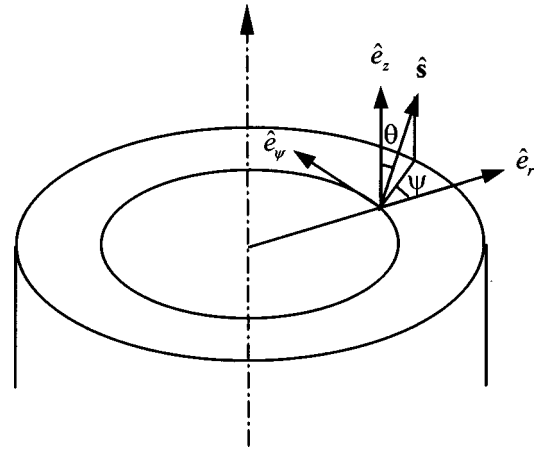


Fig. 2 Coordinates for two-dimensional axisymmetric cylinder

where μ^i , η^i , and ξ^i are the direction cosines of $\hat{\mathbf{s}}_i$ as shown in Fig. 2; and

$$\mu = \sin \theta \cos \psi \quad (9a)$$

$$\eta = \sin \theta \sin \psi \quad (9b)$$

$$\xi = \cos \theta \quad (9c)$$

Then the spectral radiative flux in \mathbf{r} and \mathbf{z} directions can be calculated from

$$q_{\lambda,r} = \sum_{i=1}^N w_i I_\lambda^i \mu^i \quad (10)$$

$$q_{\lambda,z} = \sum_{i=1}^N w_i I_\lambda^i \xi^i \quad (11)$$

and the total radiative fluxes from

$$q_r = \sum_{i=1}^M q_{\lambda_i,r} \quad (12)$$

$$q_z = \sum_{i=1}^M q_{\lambda_i,z} \quad (13)$$

where w_i is the quadrature weights associated with each direction $\hat{\mathbf{s}}_i$; N is the number of the ordinate directions; and M is the number of the wavelength bands. Based on the study of Jamaluddin and Smith [11], we choose the completely symmetric S_4 -approximation quadrature which integrates the zero, first (half and full range), and second-order moments of the intensity distribution.

2.3.2 Transformations and Discretization of RTE. Due to the diameter variation near the bottom of the glass rod, Eq. (8) is cast into the fully conservative form in a general curvilinear coordinate system (α, β)

$$\frac{\partial[rB(\mu^i \alpha_r + \xi^i \alpha_z)I_\lambda^i]}{\partial \alpha} + \frac{\partial[rB(\mu^i \beta_r + \xi^i \beta_z)I_\lambda^i]}{\partial \beta} - B \frac{\partial(\eta^i I_\lambda^i)}{\partial \psi} = \kappa_\lambda r B [n_\lambda^2 I_{b\lambda}(T) - I_\lambda^i] \quad (14)$$

where α_r , α_z , β_r , and β_z are the grid metrics and the Jacobian B is given by

$$B = \frac{\partial(\alpha, \beta)}{\partial(r, z)} = \begin{vmatrix} \alpha_r & \alpha_z \\ \beta_r & \beta_z \end{vmatrix} \quad (15)$$

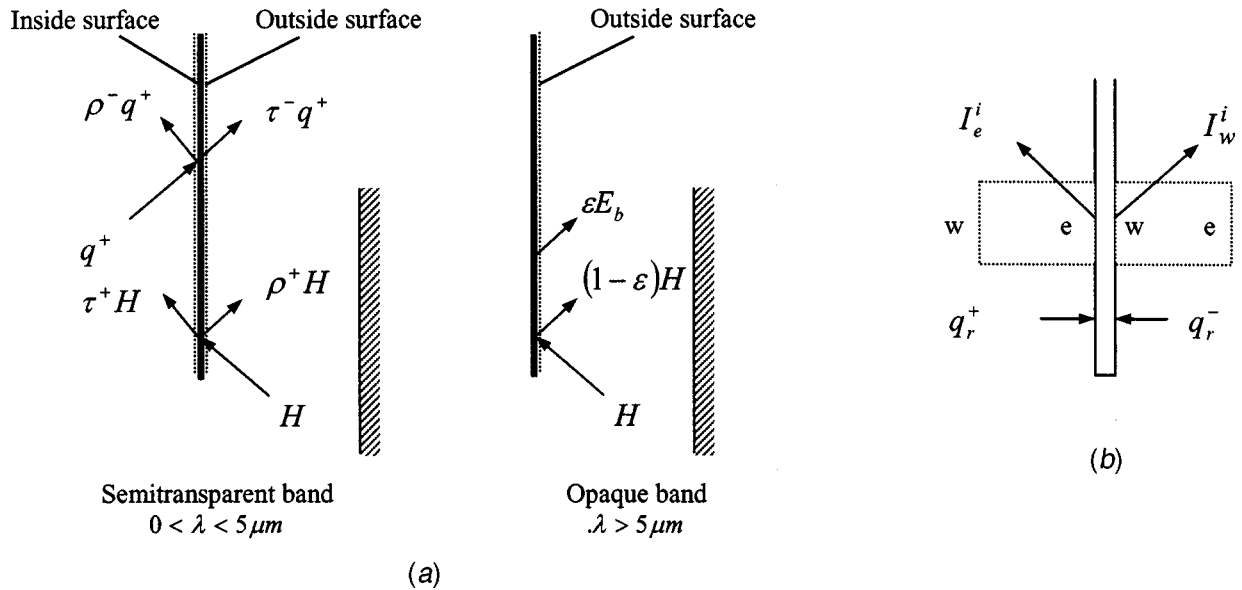


Fig. 3 Schematics illustrating the boundary conditions: (a) interface of the glass rod; and (b) gap between the two cylinders.

The angular derivative term in Eq. (14) can be discretized by using the direct differencing technique proposed by Carlson and Lathrop [15]:

$$\frac{\partial(\eta^i I_\lambda^i)}{\partial \psi} \cong \frac{s^{i+1/2} I_\lambda^{i+1/2} - s^{i-1/2} I_\lambda^{i-1/2}}{w_i} \quad (16)$$

where $i=1, 2, \dots, N_i$ for every fixed ξ . The geometrical coefficient $s^{i\pm 1/2}$ depends only on the differencing scheme, which is independent of radiative intensity and has the following recursive formula:

$$s^{i+1/2} = s^{i-1/2} + \mu^i w_i \quad (17)$$

where $s^{1/2} = 0$ when $\psi^{1/2} = 0$.

Using finite volume method to discretize the transfer Eq. (14), we have

$$\begin{aligned} & [rB(\mu^i \alpha_r + \xi^i \alpha_z) I_\lambda^i]_e - [rB(\mu^i \alpha_r + \xi^i \alpha_z) I_\lambda^i]_w \\ & + [rB(\mu^i \beta_r + \xi^i \beta_z) I_\lambda^i]_n - [rB(\mu^i \beta_r + \xi^i \beta_z) I_\lambda^i]_s \\ & - B \frac{(s^{i+1/2} I_\lambda^{i+1/2} - s^{i-1/2} I_\lambda^{i-1/2})}{w_i} \\ & = rB\kappa_\lambda (n_\lambda^2 J_{b\lambda} - I_\lambda^i) \end{aligned} \quad (18)$$

where the subscripts e , w , n , and s indicate the values in the brackets are evaluated at the eastern, western, northern and southern grid faces, respectively. In order to reduce the number of unknowns, step scheme is used to relate the intensities on the grid faces with the nodal values. This spatial differencing scheme can guarantee the intensities positive.

2.3.3 Boundary Conditions. The boundary conditions for the DOM are given below.

Symmetry of the Cylinder. The i^{th} direction along the axis of the cylinder is given by

$$r=0: \quad I_\lambda^i = I_\lambda^{i'}, \quad \mu^i = \mu^{i'} \quad (19)$$

where μ^i is the cosine of the angle between the i^{th} and the r directions.

Interface of the Glass Rod. Figures 3(a) and 3(b) illustrate the transmission and reflection at the interface of the glass rod, and at

the gap between the cylinders respectively. The assumption that the interfaces of the preform are diffuse for both transmission and reflection implies the following:

$$r=R^-: \quad I_\lambda^i = \frac{J_\lambda^-}{\pi} = \frac{\tau_\lambda^+ H_\lambda + \rho_\lambda^- q_{\lambda,r}^+}{\pi} \quad \mu^i < 0 \quad (20a)$$

$$z=0^+: \quad I_\lambda^i = \frac{J_\lambda^-}{\pi} = \frac{\tau_\lambda^+ H_\lambda + \rho_\lambda^- q_{\lambda,z}^-}{\pi} \quad \xi^i > 0 \quad (20b)$$

$$z=L^-: \quad I_\lambda^i = \frac{J_\lambda^-}{\pi} = \frac{\tau_\lambda^+ H_\lambda + \rho_\lambda^- q_{\lambda,z}^+}{\pi} \quad \xi^i < 0 \quad (20c)$$

where ξ^i is the cosine of the angle between the i^{th} direction and the z direction; the superscripts “+” and “-” refer to the quantities at the outer and inner surfaces of the cylinder respectively; τ_λ , ρ_λ , and J_λ are the diffuse transmissivity, reflectivity and radiosity respectively; $q_{\lambda,r}^\pm$, $q_{\lambda,z}^\pm$ are the one-way spectral fluxes in the glass in the r and z directions respectively; and H_λ is the irradiation on the outer surface. Similarly, the radiosities at the surfaces just outside the cylinder

$$r=R^+: \quad J_\lambda^+ = \tau_\lambda^- q_{\lambda,r}^+ + \rho_\lambda^+ H_\lambda \quad (21a)$$

$$z=0^-: \quad J_\lambda^+ = \tau_\lambda^- q_{\lambda,z}^- + \rho_\lambda^+ H_\lambda \quad (21b)$$

$$z=L^+: \quad J_\lambda^+ = \tau_\lambda^- q_{\lambda,z}^+ + \rho_\lambda^+ H_\lambda \quad (21c)$$

The one-way spectral fluxes are calculated as follows:

$$q_{\lambda,r}^+ = \sum_{i=1}^{N/2} w_i I_\lambda^i \mu^i \quad \mu^i > 0 \quad (22a)$$

$$q_{\lambda,z}^- = \sum_{i=1}^{N/2} w_i I_\lambda^i |\xi^i| \quad \xi^i < 0 \quad (22b)$$

$$q_{\lambda,z}^+ = \sum_{i=1}^{N/2} w_i I_\lambda^i \xi^i \quad \xi^i > 0 \quad (22c)$$

The irradiation H_λ is the sum of the energy contribution from all the other surfaces that include the furnace, the cylinder outer surface, and the top and bottom disk openings.

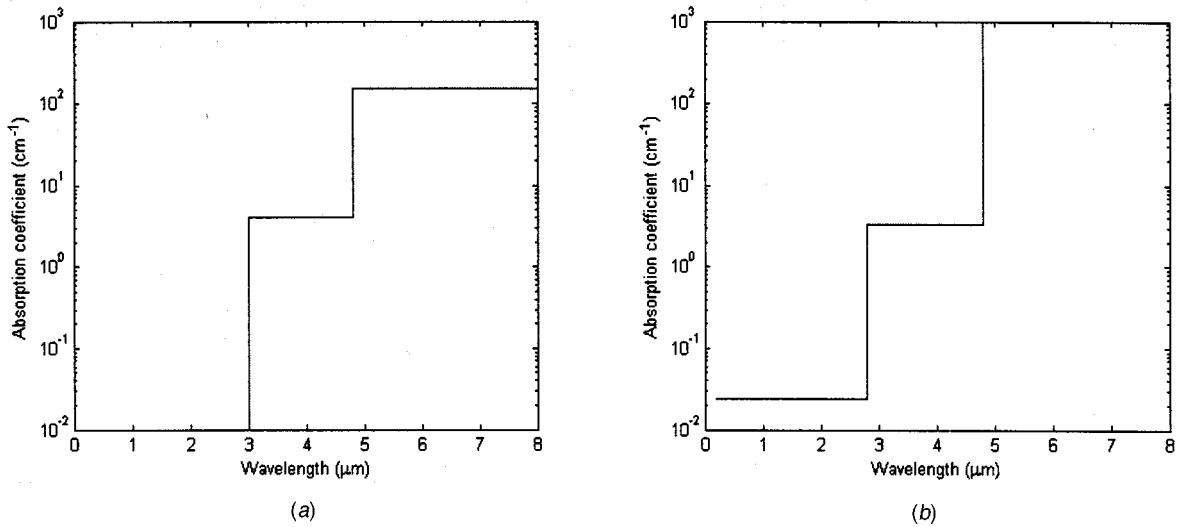


Fig. 4 Band model for absorption coefficient: (a) Myers' band model; and (b) band model used in this study.

$$H_{\lambda,i} = \sum_{j=1}^K J_{\lambda,j} F_{i-j} \quad (23)$$

where F_{i-j} is the diffuse view factor from surface element i to j . K is the total number of the surface elements. Equations (20) and (21) are for the semitransparent band. When $\lambda > 5 \mu\text{m}$ where the glass is considered to be opaque, the radiosities on the outer surface of the glass rod must be calculated from

$$J_{\lambda,i} = \varepsilon E_{b\lambda,i} + (1 - \varepsilon) H_{\lambda,i} \quad (24)$$

where ε is the emissivity of the surface; and $E_{b\lambda,i}$ is the blackbody emissive power in the i^{th} surface element. Since the furnace is opaque, its radiosities are also calculated from Eq. (24) in all the spectral range.

Gap Between the Two Cylinders. The transmission and reflection on the gap interfaces between the two cylinders should be considered:

$$I_{\lambda,e}^i = \frac{q_r^- \tau^- \tau^+ (\rho^- + \tau^- \rho^+ \tau^+) q_r^+}{\pi}, \quad \mu^i < 0 \quad (25a)$$

$$I_{\lambda,w}^i = \frac{q_r^+ \tau^- \tau^+ + (\rho^- + \tau^- \rho^+ \tau^+) q_r^-}{\pi}, \quad \mu^i > 0 \quad (25b)$$

Since the gap is very thin, it disappears when the glass melts.

2.3.4 Method of Solution. The computation of the intensity begins at the grids adjacent to the boundary surfaces along each specified direction with estimated boundary intensities and proceeds into the medium. Once the intensities in all the directions are obtained, the one-way fluxes at the boundaries are calculated and substituted into Eqs. (21a) to (21c), and the linear equations for the radiosities on the K surface elements of the outside enclosure are solved. Irradiations on the outer surface of the glass can now be calculated in Eq. (23) and are substituted into Eq. (20a) to (20c) to update the estimated inner surface radiosities. The one-way fluxes at the gap are also updated in the process. Iteration is needed for these updating processes.

The energy equation (Eq. (5)) was solved using the finite volume method with a fully implicit time marching scheme. Since the divergence of the radiative flux is strongly dependent on the temperature, an inner iteration for the temperature is carried out at each time step. The time derivative term is discretized by second-order one-sided difference scheme.

A common spatial grid is used in solving both the energy equation and the RTE. The grid is fixed on the glass rod and moves with the rod. The new position of the grid and the view factors of the glass surface are updated at each time step. In this way, there is no convection due to zone traverse since the glass does not move relative to the grid.

In this study, a uniform initial temperature of 300K was used. A sensitivity study showed that a time step of 1 second is enough for the transient problem. The grid spacing is more condensed near the bounding interfaces and the gap to account for the steep spatial change in the physical variables expected in these regions. A grid-refinement study showed that 155×37 (in z and r directions, respectively) grids is enough for the simulation.

2.4 Models of Radiative Properties. The accuracy of the solution to the RTE, or Eq. (1), depends significantly on the knowledge of the radiative properties. Specifically, care must be exercised to appropriately quantify the absorption coefficient of the glass and the reflectivity at the glass surfaces at the operating temperature.

Myers' Band Model for Spectral Absorption Coefficient. Figure 4(a) displays the Myers' bands [3] for the spectral absorption coefficient of fused silica glass. The bands commonly used in the prediction of radiative transfer in fiber drawing process are given below:

$$\kappa_\lambda = 0, \quad \lambda \leq 3 \mu\text{m};$$

$$\kappa_\lambda = 4 \text{ cm}^{-1}, \quad 3 \mu\text{m} < \lambda \leq 4.8 \mu\text{m};$$

$$\kappa_\lambda = 150 \text{ cm}^{-1}, \quad 4.8 \mu\text{m} < \lambda \leq 8 \mu\text{m};$$

Myers approximates the absorption coefficient at a small wavelength ($\lambda < 3.0 \mu\text{m}$) as zero, and consequently the radiative transfer at that band is not considered. Although the absorption coefficient is small (in the order of 0.001 to 0.3 cm^{-1}) for semitransparent glasses at this band, more than 60% of the emissive power concentrates in these shorter wavelengths for the glass at the (melting) temperature between 1000K and 2500K (see for example, blackbody emissive power spectrum in Modest [7]). Consequently, the effect of the absorption coefficient in this band on radiative transfer is considerable and cannot be neglected as will be shown in our results. It is worth noting that in Myers' band model, the absorption coefficient at the middle band ($3.0 \mu\text{m} < \lambda < 4.8 \mu\text{m}$) was based on room temperature.

Modified Absorption Band Model Used in This Study. The spectral radiative energy is negligible for short wavelengths $\lambda < 0.2 \mu\text{m}$ in the operating temperature range. In the range of $0.2 \mu\text{m} \leq \lambda < 2.8 \mu\text{m}$, taking the multiple reflections into account, the average internal transmissivity τ_i of a silica glass slab can be calculated from the tabulated data of the apparent slab reflectivity and transmissivity in (Touloukian et al. [16]). With the approximation of

$$\tau_{i,\lambda} = e^{-\kappa_\lambda d} \quad (26)$$

where d is the thickness of the slab, the average absorption coefficient for $0.2 \mu\text{m} \leq \lambda < 2.8 \mu\text{m}$ is determined to be 0.0243 cm^{-1} .

The absorption coefficients of typical glasses near the melting temperature were measured experimentally by Endrys [8] and Nijnatten et al. [9,10]; both published data suggest that the absorption coefficient in the $2.8 \mu\text{m} \leq \lambda < 4.8 \mu\text{m}$ band near melting temperature is generally 10~25% lower than that at a room temperature of 25°C. In this study, we estimate the absorption coefficient in the $2.8 \mu\text{m} \leq \lambda < 4.8 \mu\text{m}$ band to be 3.4 cm^{-1} .

For $\lambda > 4.8 \mu\text{m}$, the absorption coefficient is large and the spectral radiative flux is relatively small. Thus, the glass is considered opaque for that band. The modified band model is shown in Fig. 4(b). The optical thicknesses δ_λ for each band based on a rod radius of 4.5 cm are given as

$$\delta_\lambda = 0.1094, \quad 0.2 \mu\text{m} < \lambda \leq 2.8 \mu\text{m};$$

$$\delta_\lambda = 15.3, \quad 2.8 \mu\text{m} < \lambda \leq 4.8 \mu\text{m};$$

$$\delta_\lambda \rightarrow \infty, \quad 4.8 \mu\text{m} < \lambda;$$

Surface Reflectivity. The external surface reflectivity can be calculated from the experimentally tabulated data for the air-to-media interface by the following curve fit (Egan and Hilgeman [17]):

$$\rho^+ = -0.4399 + 0.7099 \times n_m - 0.3319 \times n_m^2 + 0.0636 \times n_m^3 \quad (27)$$

The corresponding internal surface reflectivity for any diffuse media-to-air interface is given by

$$\rho^- = 1 - \frac{(1 - \rho^+)}{n_m^2} \quad (28)$$

where n_m is the index of refraction of the medium. In this study, an average refractive index over the whole spectrum is used ($n_m = 1.42$). The consequent reflectivity and transmittivity of the external surface are 0.08 and 0.92, respectively. Those for the internal surface are 0.54 and 0.46.

3 Results and Discussions

In order to investigate the effects of the approximation methods and the models describing the glass radiative properties on the transient temperature distribution, a MATLAB program with C++ subroutines has been written to simulate the process shown in Fig. 1.

3.1 Validation. Exact integral solution of RTE is available for the one-dimensional semitransparent cylinder whose temperature and heat flux only varies in the radial direction (Kesten [18]). In order to validate our two-dimensional solution with this integral solution, the boundary conditions are modified in the codes to obtain an equivalent one-dimensional solution as follows: the diameter of the cylinder is constant; both the top and the bottom interfaces of the cylinder are assumed to be optically smooth with unity reflectivities; the temperatures in the glass and the furnace wall are assumed to be uniform so that the radiation intensity does not vary in the axial direction. Figure 5 shows comparisons of the S-4 DOM solutions and the integral solutions under different glass

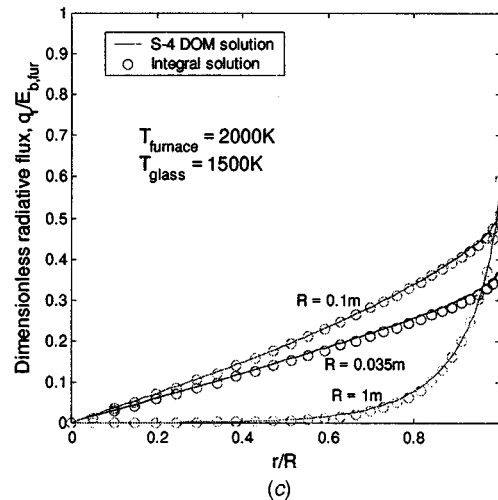
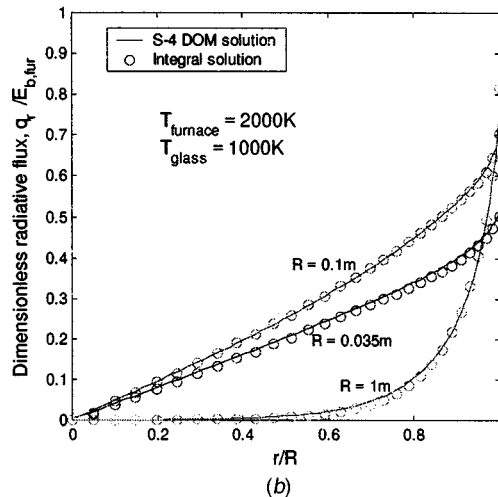
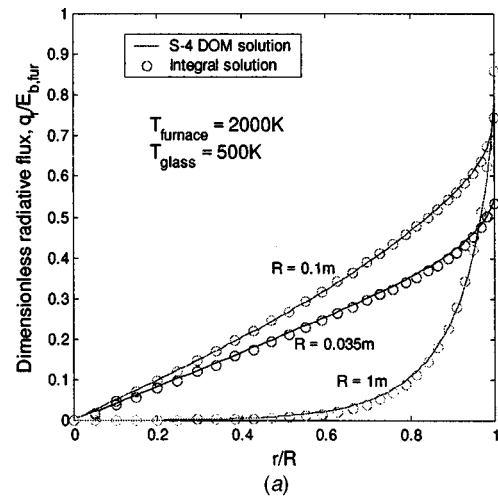


Fig. 5 Comparison of the DOM and the integral solutions (different cylinder diameters, $T_f = 2000 \text{ K}$): (a) $T_g = 500 \text{ K}$; (b) $T_g = 1000 \text{ K}$; and (c) $T_g = 1500 \text{ K}$.

temperatures and cylinder diameters. The radial flux is normalized by the furnace blackbody emissive power. As shown in Fig. 5, the computed results agree with the exact solutions.

3.2 Simulation and Discussion. In this study, we compare the following simulations:

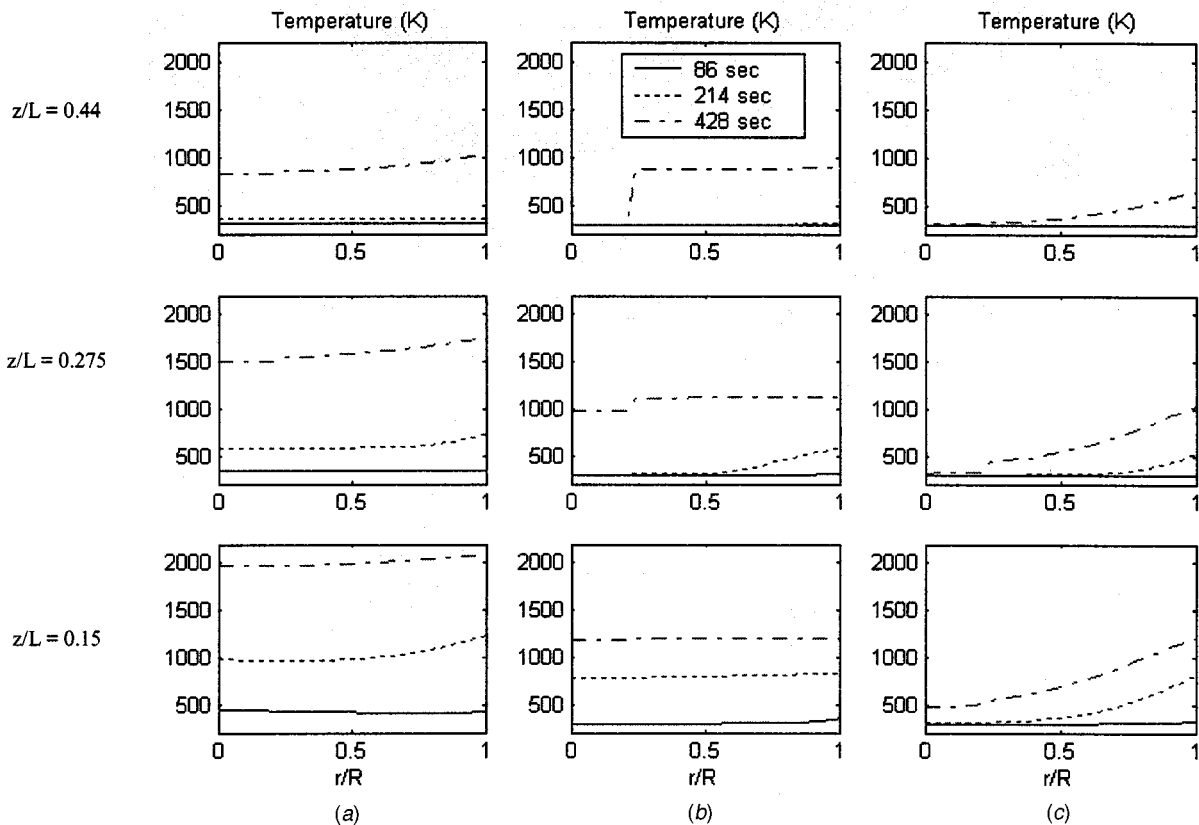


Fig. 6 Temperature distributions: (a) DOM, new band model; (b) Rosseland; and (c) DOM, Myers' band model.

1. DOM with a modified absorption band model given in Fig. 4(b)
2. RA method with the modified absorption band model
3. DOM with the Myers' band model given in Fig. 4(a).

Simulations 1 and 2 compare the effects of the optically thick assumption on the radiative transfer. Simulations 1 and 3 investigate the effects of absorption band models. Of particular interest is to compare the following:

1. The temperature distributions of the glass cylinders as displayed in Fig. 6,
2. The heat fluxes in both axial and radial directions at the tip of the gap in Fig. 7.
3. The transient temperature gradient at the tip of the gap in Fig. 8.

The values of the parameters used in the simulation are given in Table 1. The temperature distribution of the furnace is parabolic along its wall, and has a maximum value of 2400 K at the middle and a minimum value of 1500 K at both ends. The glass rod of length 0.5 m is fed with a constant speed of 0.75 mm/second into the furnace from $Z=0$ to $Z=0.5L$.

Figure 6 compares the temperature distributions at different locations and time. The total heat fluxes, which are defined in Eqs. (11–14), are compared in Fig. 7, where a positive axial flux indicates heat flowing in the positive z direction, but a positive radial flux indicates heat flowing toward the center of the rod (or negative r direction).

Effects of the Optically Thick Assumption. As shown in Fig. 6, the RA method highly underestimates the temperature due to the assumption that the glass medium is optically thick. Recall that the optical thickness is a function of both the characteristic dimension and the absorption coefficient. The followings are two causes of the error:

1. The characteristic dimension is relatively small, particularly inside the gap. These results are consistent with those in (Lee and Viskanta [5]) that was computed for glass slab; the RA underpredicts the radiative heat flux even when the thickness of the layer is larger than 1 m.
2. Although the absorption coefficient is relatively large in the middle band ($3.0 \mu\text{m} < \lambda < 4.8 \mu\text{m}$), most radiative energy concentrates in the low wavelength band that is characterized by a very small absorption coefficient of 0.0243 cm^{-1} .

Another obvious difference occurs at the gap between the cylinders. Based on several observations made in Figs. 7(a) and 7(b), the RA incorrectly predicts the heat flux as explained below:

1. When $t=86$ seconds (or $Z=0.13L$), the major portion of the glass rod is outside the furnace and thus the rod is heated mainly by the axial radiative flux from the bottom (indicated as "A" in Fig. 1). As shown in Fig. 7(a), the radial flux is negative (or flowing outward) since heat dissipates to the environment from the somewhat heated rod as expected. As a result, the radial temperature gradient at the tip of the gap is negative as reasonably predicted by the DOM with the modified band model in Fig. 8. Note that the RA underestimates the temperature and fails to predict this negative radial heat flux. Furthermore, it predicts an incorrect temperature gradient in the radial direction as shown in Fig. 8.
2. As the glass rod translates further into the furnace, the radial flux becomes positive (or flowing toward the center) and increases with r , as simulated by DOM with the modified band model, as expected. The axial flux, however, decreases with r because the view factor is larger at the center of the bottom than that at a larger radial distance. Note that since the axial flux is significantly larger than the radial flux at the tip of the gap, the temperature gradient in the radial direction

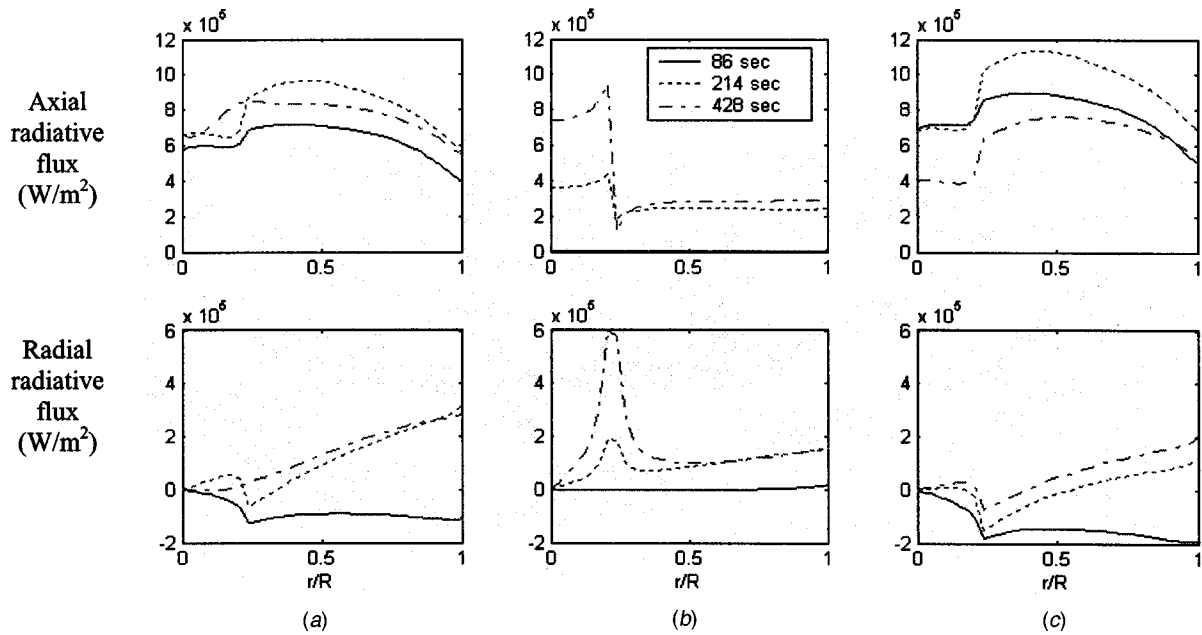


Fig. 7 Radiative flux distributions at $z/L=0.15$: (a) DOM, new band model; (b) Rosseland; and (c) DOM, Myers' band model.

is positive but small. In RA, the temperature inside the inner cylinder is underestimated. As a result, the corresponding axial temperature gradient and thus the axial heat flux is larger than that in the outer cylinder as shown in Fig. 7(b). Figure 8 shows that the temperature discontinuity in the gap results in a large positive temperature gradient at the tip of the gap. Consequently, there is a peak of radial radiative flux near the tip. The sharp drop of the temperature gradient after the temperature is elevated is due to the combination of two factors: radiative conductivity is proportional to T^3 ; the Rosseland mean absorption coefficient decreases sharply when the temperature is increased.

- It is interesting to note that the axial flux at $t=428$ is smaller than that at $t=214$ in Fig. 7(a). This is because as the glass is heated near the temperature of the furnace, the emitted flux by the glass medium is comparable to the flux from the

furnace. Thus, the net radiative flux inside the glass as the process approaches steady state is smaller than that at the initial transient.

Effects of Band Models of Absorption Coefficient. Several observations can be made in Figs. 6(c), 7(c), and 8:

- In Myers' two-step band model, the glass absorption coefficient at short wavelengths ($0.2 \mu\text{m} \leq \lambda < 2.8 \mu\text{m}$) has been neglected. As a result, the heat flux at that band is not absorbed (or attenuated) by the glass medium and thus the temperature is underestimated during the initial transient response as shown in Fig. 6(c).
- In addition, as only the radiative energy at the middle band ($3.0 \mu\text{m} < \lambda < 4.8 \mu\text{m}$) is absorbed by the glass in Myers' model that has a κ_λ more than 100 times larger than that at the short-wavelength band, the radiative flux at the middle band from the furnace is greatly attenuated along the path into the glass medium. Consequently, a very large temperature gradient is formed in the radial direction as shown in Figs. 6(c) and 8.
- The total flux in the solution using Myers' band model is somewhat larger than that using the new band model since the flux at the short wavelength band is not attenuated (absorbed) by the glass media in Myers' model.

As mentioned earlier, sufficiently large temperature gradient due to the transient heating could result in cracking at the interface and predictions of thermally induced stresses requires a good understanding of the transient temperature field and its gradient at the interface. Both Rosseland approximation and the neglect of the absorption coefficient in the $0.2 \mu\text{m} \leq \lambda < 2.8 \mu\text{m}$ band have led to erroneous prediction of temperature gradient. Most impor-

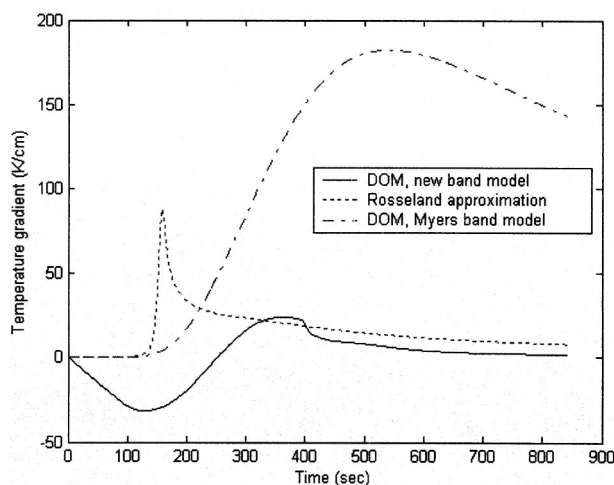


Fig. 8 Transient radial temperature gradient at the tip of the gap ($a/R=0.22$; and $d/L=0.15$).

Table 1 Parameters used in the simulation

a/R	0.22	b/L	0.15	$T_{f,\text{max}}$	2400 K
R/R_f	0.75	R/L	0.09	L/L_f	1

tantly, they fail to predict the negative temperature gradient at the earlier stage of the transient, where cracks at the joint interface are most likely.

4 Conclusions

The transient temperature and heat flux distributions in the process of heating two concentric, semitransparent glass cylinders have been presented. Specifically, we have compared two different methods in modeling the radiative transfer; namely, the discrete ordinate method and Rosseland's approximation. In addition, we have investigated the effects of the absorption coefficient at short wavelengths ($0.2 \mu\text{m} \leq \lambda < 2.8 \mu\text{m}$) on the radiative transfer, which has been neglected in the commonly used Myers' two-step band model.

Our results show that although the spectral absorption coefficient at short wavelengths is relatively small, its effects on the temperature are considerable since most of the radiative power is at this short-wavelength band under the elevated temperatures. The temperature is highly underestimated during this initial transient and its radial variation is overestimated with the Myers' band model.

The comparison between the predictions using DOM and the widely used Rosseland approximation shows that Rosseland's approximation fails miserably when the characteristic dimension is small, particularly at the gap between the cylinders even when the temperature variation is small. In addition, the assumption of optically thick must take into account the glass absorption coefficient at short wavelengths where the radiative transfer is dominant.

The solutions of the temperature field can be further used in the prediction of the thermal stress intensity near the tip of the interface which is important for the design and control of the manufacturing process.

Acknowledgments

This research has been funded by Lucent/OFS. The authors are deeply indebted to Steve Jacobs, Rob Moore, and Mahmood Tabaddor for their contribution to this manuscript.

Nomenclature

Symbols

B	= Jacobian of the curvilinear coordinates transformation
$E_{b,\lambda}$	= blackbody emissive power
G_λ	= spectral incident radiation
H_λ	= spectral irradiation in $\text{W}/(\text{m}^2 \mu\text{m})$
I_λ	= spectral radiative intensity in $\text{W}/(\text{m}^2 \mu\text{m} \text{sr})$
$I_{b\lambda}$	= spectral blackbody intensity in $\text{W}/(\text{m}^2 \mu\text{m} \text{sr})$
J_λ	= spectral radiosity in $\text{W}/(\text{m}^2 \mu\text{m})$
T	= temperature in K
k_{rad}	= radiative thermal conductivity in $\text{W}/(\text{m} \mu\text{m})$
n_λ	= spectral index of refraction
q	= total radiative heat flux in $\text{W}/(\text{m}^2)$
q_λ	= spectral radiative heat flux in $\text{W}/(\text{m}^2 \mu\text{m})$
w	= quadrature weight

Subscripts and Superscripts

e	= east side of the control volume
f	= furnace
g	= glass
n	= north side of the control volume
r	= radial coordinate direction

s	= south side of the control volume
\mathbf{n}	= normal unit vector of the surface
\mathbf{r}	= location vector
\mathbf{s}	= unit direction vector
Ω	= solid angle in sr
τ_λ	= spectral diffuse transmissivity
ρ_λ	= spectral diffuse reflectivity
κ_λ	= spectral absorption coefficient in m^{-1}
ε	= emissivity
μ^i	= cosine of the angle between the i th direction and the r direction
ξ^i	= cosine of the angle between the i th direction and the z direction
δ_λ	= optical thickness
(α, β)	= general curvilinear coordinates
w	= west side of the control volume
z	= axial coordinate direction
max	= maximum value
+	= positive coordinate direction for flux; outer surface at the interface
-	= negative coordinate direction for flux; inner surface at the interface

References

- [1] Paek, U. C., and Runk, R. B., 1978, "Physical Behavior of the Neck-Down Region During Furnace Drawing of Silica Fibers," *J. Appl. Phys.*, **49**, pp. 4417–4422.
- [2] Homay, G. M., and Walker, K., 1979, "Heat Transfer in Laser Drawing of Optical Fibers," *Glass Technol.*, **20**(1), pp. 20–26.
- [3] Myers, M. R., 1989, "A Model for Unsteady Analysis of Preform Drawing," *AIChE J.*, **35**(4), pp. 592–602.
- [4] Choudhury, S. R., Jaluria, Y., Lee, S. H.-K., 1999, "A Computational Method for Generating the Free-surface Neck-down Profile for Glass Flow in Optical Fiber Drawing," *Numer. Heat Transfer, Part A*, **35**, pp. 1–24.
- [5] Lee, K. H., and Viskanta, R., 1999, "Comparison of the Diffusion Approximation and the Discrete Ordinates Method for the Investigation of Heat Transfer in Glass," *Glass Sci. Technol. (Frankfurt/Main)*, **72**(8), pp. 254–265.
- [6] Yin, Z., and Jaluria, Y., 1997, "Zonal Method to Model Radiative Transport in an Optical Fiber Drawing Furnace," *ASME J. Heat Transfer*, **119**, pp. 597–603.
- [7] Modest, M. F., 1993, *Radiative Heat Transfer*, McGraw-Hill, NY.
- [8] Endry, Jiri, 1999, "Measurement of Radiative and Effective Thermal Conductivity of Glass," *Proc. of the 5th ESG Conf.*, A5 10–17.
- [9] Nijnatten, P. A., and Broekhuijse, J. T., 1999, "A High-Temperature Optical Test Facility for Determining the Absorption of Glass at Melting Temperatures," *Proc. of the 5th ESG Conf.*, A5 51–58.
- [10] Nijnatten, P. A., Broekhuijse, J. T., and Faber, A. J., 1999, "Spectral Photon Conductivity of Glass at Forming and Melting Temperatures," *Proceedings of the 5th ESG Conference*, A5 2–9.
- [11] Jamaluddin, A. S., and Smith, P. J., 1988, "Predicting Radiative Transfer in Axisymmetric Cylindrical Enclosures Using the Discrete Ordinates Method," *Combust. Sci. Technol.*, **62**, pp. 173–186.
- [12] Lee, K. H., and Viskanta, R., 1997, "Prediction of Spectral Radiative Transfer in A Condensed Cylindrical Medium Using Discrete Ordinates Method," *J. Quant. Spectrosc. Radiat. Transf.*, **58**, pp. 329–345.
- [13] Chung, K. B., Moon, K. M., and Song, T. H., 1999, "Treatment of Radiative Transfer in Glass Melts: Validity of Rosseland and P-1 Approximations," *Phys. Chem. Glasses*, **40**, pp. 26–33.
- [14] Viskanta, R., and Anderson, E. E., 1975, "Heat Transfer in Semitransparent Solids," *Adv. Heat Transfer*, **11**, pp. 317–441.
- [15] Carlson, B. G., and Lathrop, K. D., 1968, "Transport Theory—The Method of Discrete Ordinates," *Computing Methods in Reactor Physics*, H. Greenspan, C. N. Kelber, and D. Okrent, eds., Gordon & Breach, New York, pp. 165–266.
- [16] Touloukian, Y. S., DeWitt, D. P., and Hertzberg, R. S., eds., 1973, *Thermal Radiative Properties: Nonmetallic Solids*, **8** of Thermophysical Properties of Matter, Plenum Press, New York, pp. 1569–1576.
- [17] Egan, W. G., and Hilgeman, T. W., 1979, *Optical Properties of Inhomogeneous Materials: Applications to Geology, Astronomy, Chemistry and Engineering*, Academic Press, New York.
- [18] Kesten, Arthur S., 1968, "Radiant Heat Flux Distribution in a Cylindrically-Symmetric Nonisothermal Gas With Temperature-Dependent Absorption Coefficient," *J. Quant. Spectrosc. Radiat. Transf.*, **8**, pp. 419–434.